JOC The Journal of Organic Chemistry

Article

pubs.acs.org/joc

A Nonempirical Approach for Direct Determination of the Absolute Configuration of 1,2-Diols and Amino Alcohols Using Mg(II)bisporphyrin

Sk Asif Ikbal, Avinash Dhamija, Sanfaori Brahma, and Sankar Prasad Rath*

Department of Chemistry, Indian Institute of Technology Kanpur, Kanpur 208016, India

Supporting Information

ABSTRACT: We report here a simple, facile, and direct nonempirical protocol for determining the absolute stereochemistry of a variety of chiral 1,2-diols and amino alcohols at room temperature with no chemical derivatization using Mg(II)bisporphyrin as a host. Addition of excess substrates resulted in the formation of a 1:2 host−guest complex in which two substrates bind in an unusual *endo-endo* fashion because of interligand H-bonding within the bisporphyrin cavity leading to the formation of a unidirectional screw in the bisporphyrin moiety that allowed us an accurate absolute stereochemical determination of the chiral substrate via exciton-coupled circular dichroism (ECCD). The sign of the CD couplet has also been found to be inverted when the stereogenic center is moved by one C atom simply from the bound to an unbound functionality and thus able to discriminate between them successfully. Strong complexation of the alcoholic oxygen with Mg(II)bisporphyrin rigidifies the host−guest complex, which eventually enhances its ability to stereochemically differentiate the asymmetric center. The ECCD sign of a large number of substrates has followed consistent and predictable trends; thus, the system is widely applicable. Moreover, computational calculations clearly support the experimental observations along with the absolute stereochemistry of the chiral substrate.

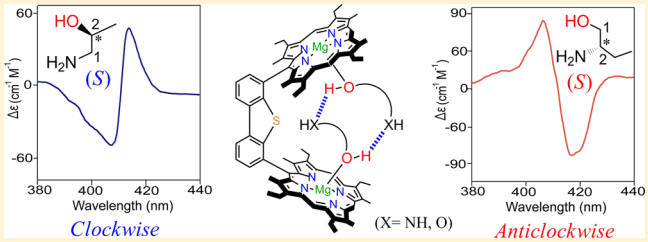

INTRODUCTION

The assignment of the absolute stereochemistry of chiral molecules remains a very important topic in the chemical and biological world today.[1−5] Hydrogen bonding plays an important role in determining the three-dimensional structures adopted by proteins and nucleic bases. For example, the double-helical structure of DNA is largely due to the hydrogen bonding interactions between its base pairs, which link one complementary strand to the other and permit replication.[6] Exciton-coupled circular dichroism (ECCD) is one of the most popular, effective, and nonempirical methods of stereochemical characterization of the chiral substrates. Upon formation of a chiral host−guest supramolecular complex between an achiral bis-metalloporphyrin derivative and a chiral substrate, a supramolecular helical system that produces a bisignate CD curve (so-called exciton couplet) in the porphyrin spectral region that allows the determination of the guest's absolute stereochemistry is generated.[7−12] A large number of substrates, such as alcohols,[13] amines,[13] diols,[14a−c] epoxides,[14d] and carboxylic acids,[15] have been explored previously, where chemical derivatization of the functional groups, in most cases, is required to bind in a 1:1 host−guest complexation with Zn-porphyrin *tweezers*. As a result, the sign of the resultant ECCD couplet reflects the helicity of the interacting chromophores and consequently the chirality of the derivatives only. Recently, Borhan et al. showed chiral sensing for the 1:1 host−guest complex for a series of chiral carboxylic acid derivatives in which the stereocenter is away from the binding site.[15a]

Porphyrin *tweezers* have been used to determine the stereochemistry of chiral substrates for a long time.[7,8,10] However, the addition of excess substrate and/or the presence of a bulky substituent often leads to a change in stoichiometry from a 1:1 to 1:2 host−guest complex that, however, would diminish the CD intensity along with inversion of the sign in most cases.[8] Another problematic issue was the weak binding of an alcoholic substrate with the zinc(II) center, which also results in an inconsistent trend in the predicted ECCD couplets in most cases.[14] Thus, developing a practical method for unequivocally determining the chirality of the 1,2-diols and amino alcohols has remained one of the most challenging tasks.[14]

In this investigation, a rigid Mg(II)bisporphyrin has been successfully utilized as a host, which allows an accurate determination of the absolute configuration directly for a series of 1,2-diols and amino alcohols having one or two chiroptic centers without any need for functional derivatization. Strong complexation of the alcoholic oxygen with Mg(II)bisporphyrin would rigidify the supramolecular complex and thus enhance the scope of possible stereochemical differentiation in the asymmetric center.

Received: April 13, 2016
Published: May 27, 2016

DOI: 10.1021/acs.joc.6b00724
J. Org. Chem. 2016, 81, 5440−5449

Scheme 1. Synthetic Outline of the Complexes and Their Abbreviations

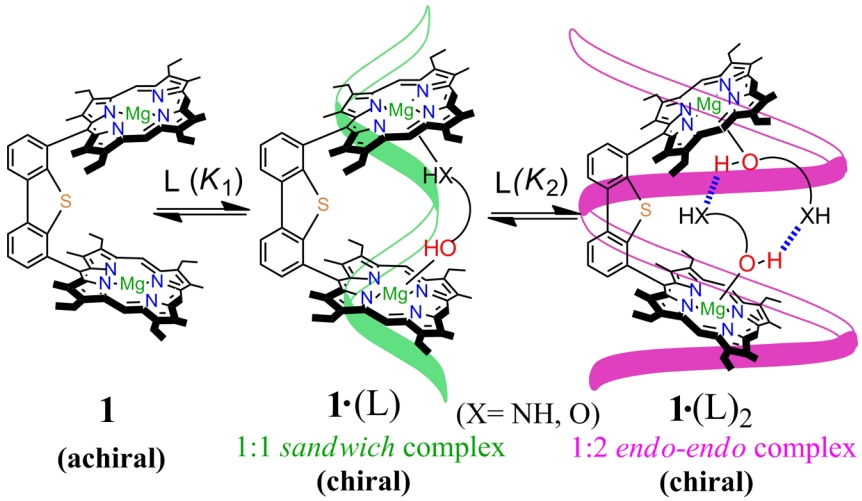

Addition of excess substrate to a dibenzothiophene-bridged Mg(II)bisporphyrin resulted in the formation of 1:2 host−guest complexes in which two substrates bind in an unusual *endo-endo* fashion within the bisporphyrin cavity, leading to the formation of unidirectional screw that allows the absolute stereochemical determination of the chiral substrate based on the observed ECCD. Such binding of the substrate, interlocked by the interligand H-bonding interaction, generates a more sterically sensitive binding cavity that even enhances the CD signal intensity. Also, a facile protocol has been reported here by which one can even discriminate the site of the stereogenic center between bound and unbound functionality with effective helix inversion, which is one of the most challenging tasks in supramolecular chirogenesis. Spectroscopic investigations, including single-crystal X-ray structure determination and extensive density functional theory (DFT) studies, have allowed us to rationalize systematically the origin of the optical activity unambiguously in a series of 1:2 host−guest complexes that leads to the absolute stereochemical determination of a large number of chiral substrates. We have recently reported briefly the X-ray structure of a 1:2 complex with (1*S*,2*S*,3*R*,5*S*)-2,3-pinanediol in a preliminary communication.[10b]

RESULTS AND DISCUSSION

Dibenzothiophene-bridged Mg(II)bisporphyrin [**1** (Scheme 1)] has been synthesized using a procedure reported previously.[16] The interaction of **1** with chiral 1,2-diol/amino alcohol L (Scheme 2) as a substrate was first studied by UV−visible spectroscopy (Figure S1). At a low substrate concentration, 1:1 *sandwich* complex was formed, which is characterized by a gradual decrement accompanied by a bathochromic shift of Soret and shoulder bands. However, addition of excess substrate to **1** results in the red shift of the Soret and Q bands along with a slight increase in Soret band intensity due to the formation of the 1:2 host−guest complex. All the 1:2 host−guest complexes reported here have been isolated as solids and spectroscopically characterized including single-crystal X-ray structure determination of three representative complexes. The synthetic outline of the complexes and their abbreviations are shown in Scheme 1, while detailed synthetic procedures and their characterizations are given in the Experimental Section. Similar to the diols/amino alcohols, a series of chiral monoalcohol/amines [$L^{20}_{(S)}$−$L^{24}_{(S)}$ (Scheme S1)] with similar structures have also been employed to bind with **1**.

Job's continuous-variation plot between the host (**1**) and substrates (L) would be quite helpful in determining the stoichiometry of the complex in solution, which has been performed using CD spectroscopic studies. It has been found that, in the low-concentration region of the substrate, maximal changes in the CD amplitudes were found at a molar ratio of 0.5, indicating 1:1 host−guest complexation (Figure S2), which is converted to 1:2 at higher substrate concentrations. However, for substrates with a bulky substituent, optimal formation of the complex was found at molar ratios of 0.33, indicating direct formation of the 1:2 host−guest complex (Figure S3). ESI mass spectroscopy also confirms the formation of 1:2 host−guest complexes (Figure S4). The ^{1}H NMR spectrum plays an important role in determining the structure of the complex in solution (Figures S5−S20). The guest ligand protons have experienced large upfield shifts because of substrate capture within the bisporphyrin cavity in the host−guest complex.

X-ray structures of **1**·($L^{7}_{(S)}$)$_2$ and **1**·($L^{10}_{(S)}$)$_2$ have been reported here, while the structure of **1**·($L^{15}_{(2S,3R)}$)$_2$ was recently reported by us in a preliminary communication.[10b] The molecules are crystallized in the chiral space groups, and the structural and bonding parameters are compared in Table 1. The substrate binds to the magnesium center in an *endo-endo* fashion through oxygen atoms as observed in the crystal structure (Figure 1 and Figure S21), while the thermal ellipsoid plots and molecular packing are displayed in Figures S22−S27. In each molecule, two porphyrin macrocycles are adapted to hold the substrates inside its scaffold by adjusting their Mg···Mg distance to ∼8.0 Å. Each Mg(II) center acquires five-coordinate square-pyramidal geometry and is displaced by ∼0.35 Å from the mean planes of the $C_{20}N_4$ porphyrinato core. The presence of two strong OH···NH_2 (for amino alcohols) and three OH···OH (for diols) interligand H-bonds (Table 1) prevents the free movement of the substrates within the bisporphyrin cavity and hence interlocks the two porphyrin rings in a stereospecific way. The induction of the asymmetric information from the enantiopure chiral substrate is clearly reflected in the unidirectional screw that is observed in the X-ray structure of the host−guest complex.

There are two molecules (Figure S21) in the asymmetric unit of **1**·($L^{10}_{(S)}$)$_2$ that, however, have different structural and

DOI: 10.1021/acs.joc.6b00724
J. Org. Chem. 2016, 81, 5440−5449

Scheme 2. Chiral 1,2-Diols and Amino Alcohols (L) Used

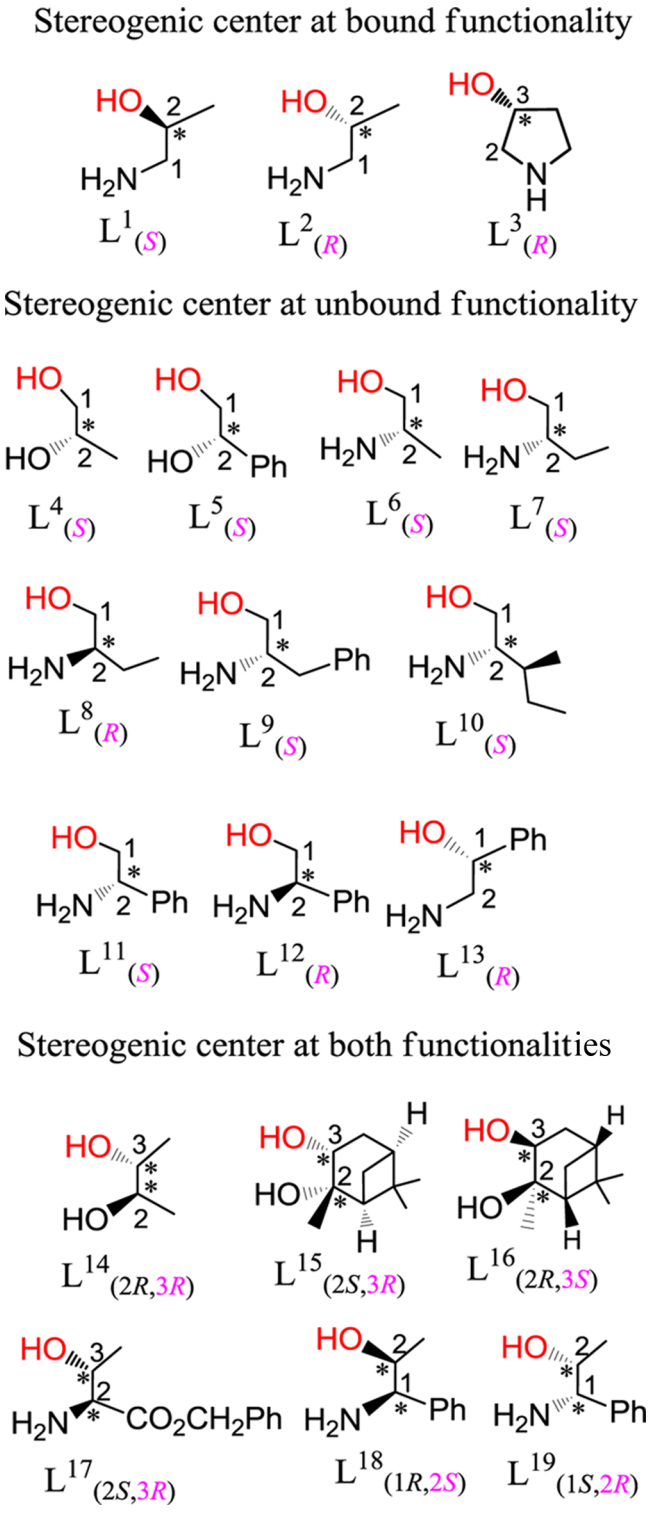

geometrical parameters. The average Mg–N_p distances are different between two molecules: 2.084(8) Å for molecule I and 2.073(8) Å for molecule II. The Mg–O_{ax} distances are also different; distances of 2.066(6) and 2.074(6) Å are observed in molecules I and II, respectively. The projection of the binding site at the chiral center forced two porphyrin macrocycles to be twisted around the rigid dibenzothiophene bridge to minimize the host–guest steric interaction that has resulted in torsion angles (Mg1–C33–C33A–Mg2) (Φ) of +3.94° for **1**·($L^{7}_{(S)}$)$_2$, −0.72° (molecule I) and +1.52° (molecule II) for **1**·($L^{10}_{(S)}$)$_2$, and −3.84° for **1**·($L^{15}_{(2S,3R)}$)$_2$.

The interaction of chiral substrate L with **1** was also monitored in dichloromethane at 295 K using CD spectroscopy. The binding constants have been determined by using the data obtained from the CD spectroscopic titration (Table S1 and Figures S28–S53). Two sets of spectral data were analyzed with HypSpec (Protonic Software),[17] considering a binding model with three colored stoichiometric states of **1**, the 1:1 *sandwich* complex, and the 1:2 *endo-endo* complex (Scheme 1). It has been observed that 1,2-diols bind stronger than amino alcohols as magnesium has a greater affinity for the oxygen atom.

The CD spectra of 1:2 *endo-endo* complexes have been calculated using CD titration data. It has also been observed that the CD intensity increases with an increase in the bulk of the substituents of the substrate, although after some critical volume, the intensity again decreases as the *endo-endo* forms become increasingly unstable because of strong steric interaction. Again, diol produces a CD signal stronger than that of the amino alcohol as diol forms stronger H-bonding interactions. Table 2 and Table S1 compare the spectral values of 1:2 *endo-endo* complexes reported here.

Complete reversal of the bisignate CD signals has been observed just by changing the handedness of the enantiomeric substrate (Figure 2A and Figure S54), which demonstrates the full and unambiguous rationalization of the chirality transfer processes from the chiral substrate to the achiral host. Interestingly, enantiopure monoalcohol/amines [$L^{20}_{(S)}$–$L^{24}_{(S)}$] also bind to **1** to produce 1:2 *endo-endo* complexes only but do not generate any chiroptical response (Figure S55) because they cannot produce the intersubstrate H-bonding that is the key element for stabilizing the *endo-endo* conformer.

In general, 1:2 host–guest complexes show weak or negligible CD intensity because of monotopic binding of the substrate with the host. In sharp contrast, highly enhanced bisignate CD signals are obtained for the 1:2 *endo-endo* complexes reported here, which is due to the formation of unidirectional twist in the *endo-endo* conformation stabilized by the interligand H-bonding. The absence of such H-bonding leads to the stabilization of the *exo-endo* conformer (*vide infra*), resulting in a negligible chirogenic response as also observed with enantiopure monoalcohol/monoamine. After detailed scrutiny of the CD signals observed for the 1:2 *endo-endo* complexes (Table 2), the substrates can be divided into three groups: (A) the substrate [$L^{1}_{(S)}$–$L^{3}_{(R)}$ and $L^{14}_{(2R,3R)}$–$L^{19}_{(1S,2R)}$] with a stereogenic center at the bound functionality, (B) the substrate [$L^{4}_{(S)}$–$L^{13}_{(R)}$] with the stereogenic center at the unbound functionality, and (C) the substrate with the stereogenic centers at both bound and unbound functionalities [$L^{14}_{(2R,3R)}$–$L^{19}_{(1S,2R)}$].

As can be seen with group A substrates, the *S* ligand shows a positive CD couplet while the *R* ligand produces a negative CD couplet in the 1:2 *endo-endo* complexes. Interestingly, complete reversal of the CD couplets has been observed with group B substrates in which the stereogenic center has moved just one carbon atom from a bound to an unbound functionality. This has been reflected in the opposite chiroptic responses observed between **1**·($L^{1}_{(S)}$)$_2$ and **1**·($L^{7}_{(S)}$)$_2$ and between **1**·($L^{2}_{(R)}$)$_2$ and **1**·($L^{8}_{(R)}$)$_2$ (Figure 2B,C). However, when the stereogenic centers are present at both bound and unbound functionalities, the sign of the CD couplet is decided by the stereogenic center at the bound functionality (Figure 2D) only.

DOI: 10.1021/acs.joc.6b00724
J. Org. Chem. 2016, 81, 5440–5449

Table 1. Selected X-ray Structural Parameters

complex			Mg−N_p[a]	Mg−O_{ax}[a]	Δ^{Mg}_{24}[b]	θ[c]	Mg···Mg[a]	O(H)···N/O[d]	torsion angle (Φ)[e]
1·($L^{7}_{(S)}$)$_2$		core I	2.082(4)	2.069(3)	0.35	44.9	7.99	2.727(4), 2.748(5)	+3.94
		core II	2.084(2)		0.36				
1·($L^{10}_{(S)}$)$_2$	molecule I	core I	2.085(8)	2.066(6)	0.35	42.8	7.98	2.698(10), 2.741(10)	−0.72
		core II	2.083(8)		0.34				
	molecule II	core I	2.074(8)	2.074(6)	0.34	42.8	8.00	2.725(10), 2.679(10)	+1.52
		core II	2.072(8)		0.36				
1·($L^{15}_{(2S,3R)}$)$_2$		core I	2.085(3)	2.069(3)	0.44	40.2	8.02	2.747(3), 2.938(3), 2.842(3)	−3.84
		core II	2.088(3)		0.36				

[a]Average value in angstroms. [b]Displacement of Mg in angstroms from the least-squares plane of the $C_{20}N_4$ porphyrinato core. [c]Angle between two least-squares planes of the $C_{20}N_4$ porphyrinato core. [d]H-Bonding distances in angstroms. [e]Mg1−C33−C33A−Mg2 torsion angle.

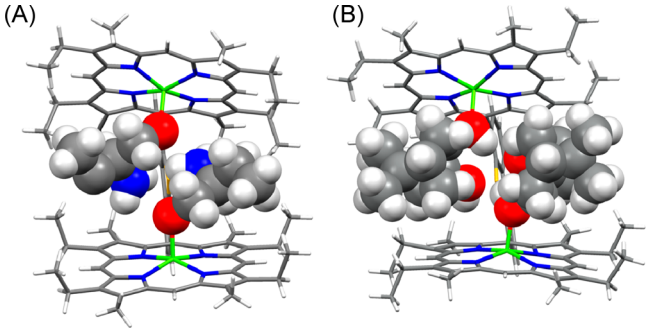

Figure 1. Molecular structures (at 100 K) of (A) **1**·($L^{7}_{(S)}$)$_2$ and (B) **1**·($L^{15}_{(2S,3R)}$)$_2$. Guest ligands are shown as space-filling models.

Molecular recognition of the bisporphyrin host for guest ligands would require high structural and binding site complementarity between the host and the guest.[18] It is now necessary to understand why dibenzothiophene-bridged Mg(II)bisporphyrin stabilizes 1:2 host−guest complexes in which two substrates bind in an unusual *endo-endo* fashion. There are two binding sites available for a guest, one is inside and the other outside the bisporphyrin cavity.[19] This leads to the formation of three types of binding motifs, viz., *endo-endo*, *exo-endo*, and *exo-exo* (Scheme 3). Geometry optimizations of all three possible conformations have also been performed, and their energies are compared in Figure S56. As can be seen, the *endo-endo* form is highly stabilized between **1** and $L^{10}_{(S)}$ compared to the *exo-endo* and *exo-exo* forms by 30.62 and 36.52 kcal mol^{-1}, respectively. The interligand H-bonding, which is present in the *endo-endo* form only, has contributed such stabilization as compared to that in the *endo-exo* and *exo-exo* forms. This is further supported by the fact that the *exo-endo* form is the most stable one rather than the *endo-endo* form when the unbound -NH_2 group is replaced with a -CH_3/SH group in which the interligand H-bonding is very weak if not impossible (Figures S57 and S58). In the absence of intersubstrate H-bonding, the stability of the complex decreases in the following order: *exo-endo* > *endo-endo* > *exo-exo*. Theoretical studies have also been performed using $L^{15}_{(2S,3R)}$ (Figures S59−S61), which, however, provided similar results.

The induction of the asymmetric information from the enantiopure chiral substrate is clearly reflected in the unidirectional screw that is observed in the X-ray structure of the *endo-endo* complex. Because of the spacer's rigidity, two porphyrin rings have little flexibility in the 1:2 *endo-endo* complexes, which however generates a small torsional (Mg1−C33−C33A−Mg2) angle (Φ). The projection of the binding site at the chiral center (*R*) of $L^{15}_{(2S,3R)}$ induces an anticlockwise

Table 2. CD Spectral Data of 1·$(L)_2$ in Dichloromethane at 295 K[a]

substrate (L)	predicted sign	λ (nm) [$\Delta\varepsilon$ (M^{-1} cm^{-1})][b]	A_{cal}[b]
Stereogenic Center at the Bound Functionality			
$L^{1}_{(S)}$	positive	415 [55]	+94
		406 [−39]	
$L^{2}_{(R)}$	negative	416 [−47]	−89
		406 [42]	
$L^{3}_{(R)}$	negative	417 [−72]	−112
		405 [40]	
Stereogenic Center at the Unbound Functionality			
$L^{4}_{(S)}$	negative	416 [−60]	−90
		405 [30]	
$L^{5}_{(S)}$	negative	416 [−121]	−232
		405 [111]	
$L^{6}_{(S)}$	negative	417 [−42]	−82
		406 [40]	
$L^{7}_{(S)}$	negative	417 [−85]	−164
		406 [79]	
$L^{8}_{(R)}$	positive	417 [85]	+160
		406 [−75]	
$L^{9}_{(S)}$	negative	420 [−48]	−92
		408 [44]	
$L^{10}_{(S)}$	negative	423 [−42]	−78
		407 [36]	
$L^{11}_{(S)}$	negative	422 [−31]	−76
		408 [45]	
$L^{12}_{(R)}$	positive	422 [37]	+77
		408 [−40]	
$L^{13}_{(R)}$	positive	413 [27]	+49
		403 [−22]	
Stereogenic Centers at Both Functionalities			
$L^{14}_{(2R,3R)}$	negative	416 [−118]	−188
		406 [70]	
$L^{15}_{(2S,3R)}$	negative	418 [−117]	−215
		407 [98]	
$L^{16}_{(2R,3S)}$	positive	419 [118]	+219
		407 [−101]	
$L^{17}_{(2S,3R)}$	negative	418 [−40]	−74
		408 [34]	
$L^{18}_{(1R,2S)}$	positive	418 [45]	+80
		406 [−35]	
$L^{19}_{(1S,2R)}$	negative	418 [−47]	−83
		407 [36]	

[a]A large excess of substrate was used to obtain the maximal change in CD. [b]A_{cal} (=$\Delta\varepsilon_1$ − $\Delta\varepsilon_2$) represents the total amplitude of the calculated CD couplets.

DOI: 10.1021/acs.joc.6b00724
J. Org. Chem. 2016, 81, 5440−5449

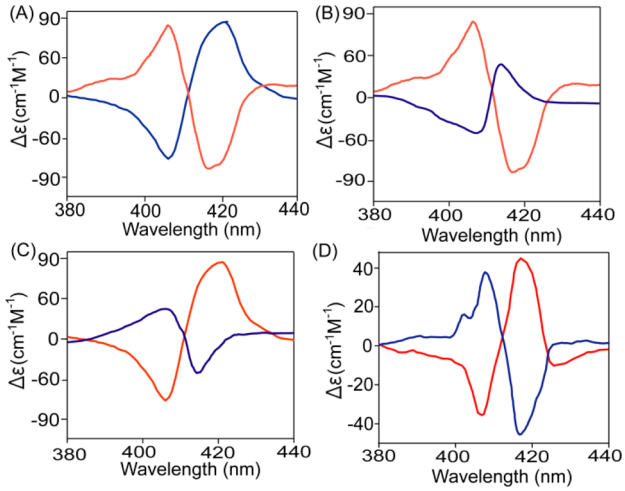

Figure 2. CD spectra of (A) **1**·$(L^{7}_{(S)})_2$ (red) and **1**·$(L^{8}_{(R)})_2$ (blue), (B) **1**·$(L^{1}_{(S)})_2$ (blue) and **1**·$(L^{7}_{(S)})_2$ (red), (C) **1**·$(L^{2}_{(R)})$ (blue) and **1**·$(L^{8}_{(R)})_2$ (red), and (D) **1**·$(L^{18}_{(1R,2S)})_2$ (red) and **1**·$(L^{19}_{(1S,2R)})_2$ (blue).

Scheme 3. Possible Binding Motifs (*endo-endo*, *exo-endo*, and *exo-exo*)

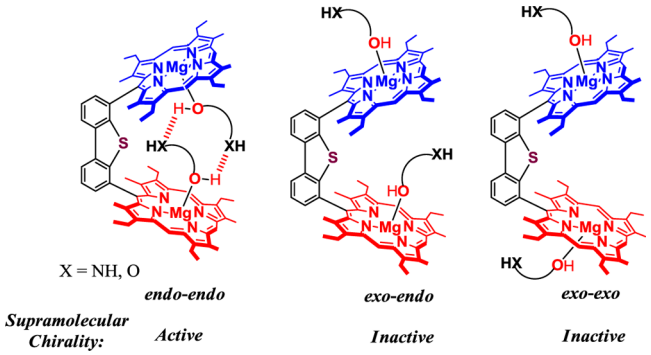

twist of the bisporphyrin around the rigid dibenzothiophene bridge with a torsion angle (Φ) of −3.84° to minimize the host−guest steric interactions, which also resulted in the negative sign of the CD signal in solution (Table 2 and Table S1). However, a torsion angle (Φ) of +3.94° observed for **1**·$(L^{7}_{(S)})_2$ fails to support the negative CD couplet obtained in solution (*vide supra*). A computational study has revealed stabilization of the anticlockwise twisted host−guest complex and therefore supports the observation of a negative CD signal for the complex in solution (*vide infra*). Such a small positive torsional angle (of +3.94°) observed in the X-ray structure might be, therefore, due to a crystal packing (Figure S62) effect (arises from π−π interactions between two adjacent and nearly coplanar porphyrin rings in the crystal lattice) present in the solid that would not contribute in solution and thus produces the negative sign of the CD signal. This has been clearly reflected in the observed CD inversion between the solid and solution phases (Figure S63) of the complex. Single-point energy calculations of two adjacent bisporphyrin molecules have been performed with the help of the DFT method in which the π−π interactions give stability by 27.23 kcal/mol. In **1**·$(L^{10}_{(S)})_2$, however, two molecules that have opposite directions of twisting are present in the asymmetric unit (X-ray structure). DFT calculation of the complex has shown the stabilization of the anticlockwise twisted form (*vide infra*) that eventually would display a negative sign for the CD signal in solution as observed in the experiment.

DFT optimizations provided more insight into the directionality of the twisting of two porphyrins in the 1:2 host−guest complexes (Figure 3, Figures S64−S71, and Table S2). The preexisting chirality of the substrate has forced two porphyrin macrocycles to be oriented in a stereospecific direction to minimize host−guest steric interactions in which the *S* substrate shows a positive CD couplet while the *R* substrate produces a negative CD couplet in the 1:2 *endo-endo* complex. It is, however, interesting to note that even if two macrocycles are twisted manually in opposite directions, the optimized structure stabilizes only one conformer. The TDDFT method is used to produce a theoretical CD spectrum, which has a sign identical with that of the experimental CD signal (Figure 4 and Figure S72).

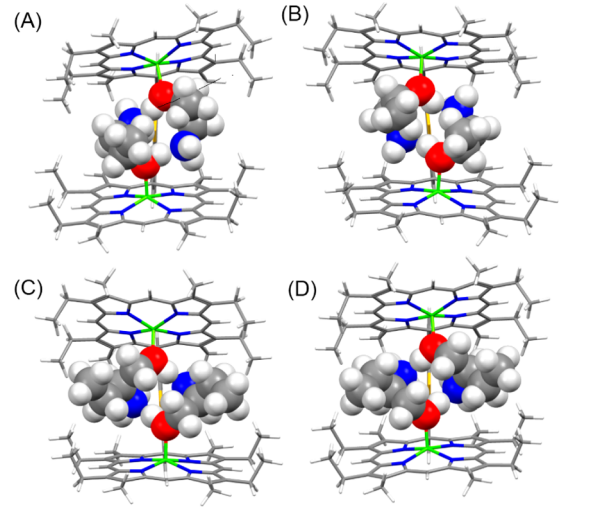

Figure 3. B3LYP/6-31G+(d,p)-optimized geometries of (A) **1**·$(L^{1}_{(S)})_2$, (B) **1**·$(L^{2}_{(R)})_2$, (C) **1**·$(L^{7}_{(S)})_2$, and (D) **1**·$(L^{8}_{(R)})_2$. Guest ligands are shown as space-filling models.

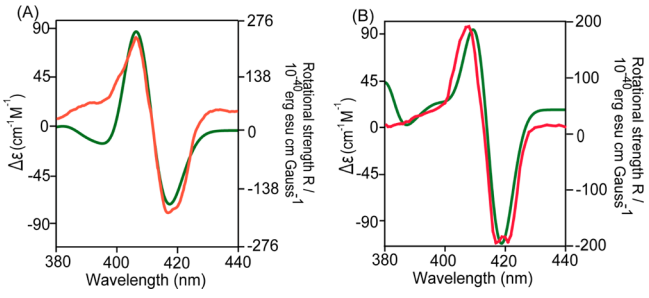

Figure 4. TDDFT-calculated CD spectrum (green line) and experimental CD spectrum (red line) of (A) **1**·$(L^{7}_{(S)})_2$ and (B) **1**·$(L^{15}_{(2S,3R)})_2$.

To visualize the chirality induction process pictorially, a working model (Figure 5) based on the experimental (X-ray structure) and theoretical investigation has been demonstrated here. To derive correlation between the observed ECCD and the low-energy conformation, we have performed conformational analysis with all of the possibilities and evaluated the conformations with the lowest energy (Figures S73 and S74). (*S*)-Amino alcohol, $L^{1}_{(S)}$, is taken as an example in which the

DOI: 10.1021/acs.joc.6b00724
J. Org. Chem. 2016, 81, 5440−5449

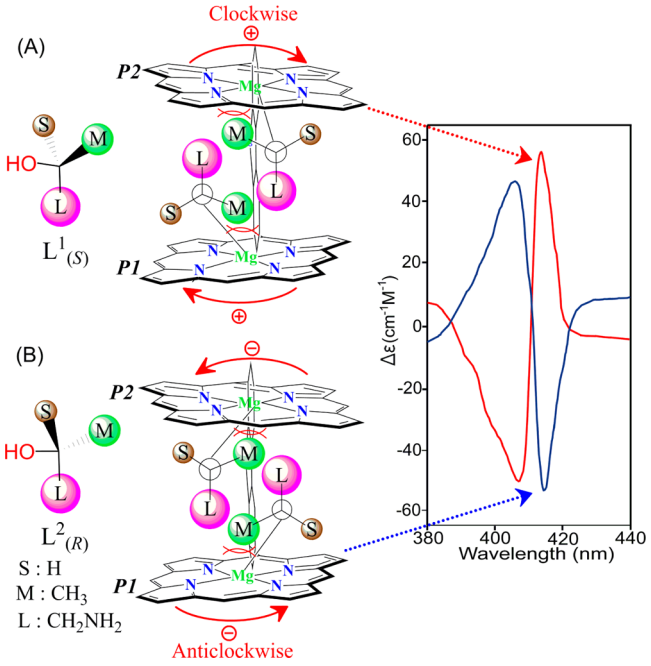

Figure 5. Working model for the 1:2 *endo-endo* complex correlating the helicity of the interacting chromophores with the observed CD couplets of (A) **1**·$(L^1_{(S)})_2$ and (B) **1**·$(L^2_{(R)})_2$. Here the stereogenic center is at the bound functionality. The peripheral substituent on the porphyrin ring has been omitted for the sake of clarity.

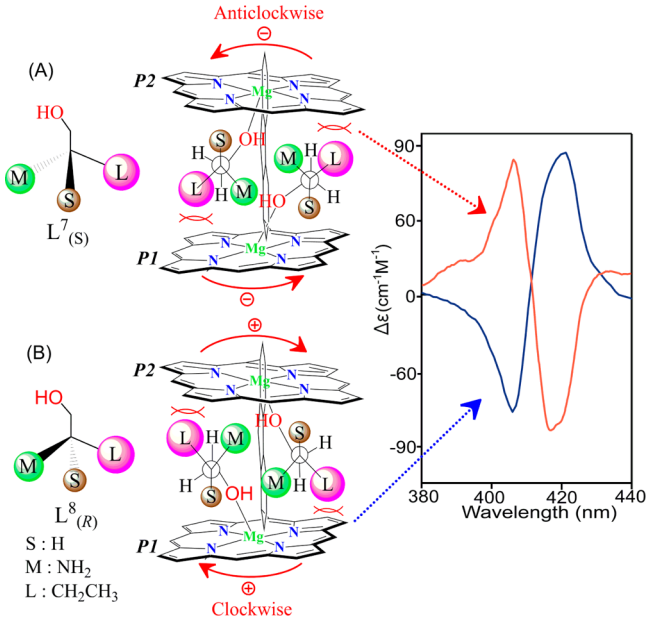

Figure 6. Working model for the 1:2 *endo-endo* complex correlating the helicity of the interacting chromophores with the observed CD couplets of (A) **1**·$(L^7_{(S)})_2$ and (B) **1**·$(L^8_{(R)})_2$. Here the stereogenic center is at the unbound functionality. The peripheral substituent on the porphyrin ring has been omitted for the sake of clarity.

stereogenic center is at the bound functionality. The 1:2 *endo-endo* complex **1**·$(L^1_{(S)})_2$ produces a positive CD sign in solution, which is supported by DFT. The chiral amino alcohol is represented by the Newman projection where the stereogenic center is at the front and the oxygen atom of the hydroxyl group is at the back. According to the model, the host porphyrin (***P1***) approaches the binding site (-OH) from the side of the medium, M (CH_3), and small, S (H), groups, keeping the large group, L (CH_2NH_2), at the opposite side. Now the host porphyrin (***P1***) will slide away from the large (L) to medium (M) to small (S) groups based on their relative size[20] to minimize the host–guest steric interactions. As a result, two porphyrin rings are twisted in a clockwise direction, which results in positive CD couplets. Similarly, the *R* enantiomer $L^2_{(R)}$ gives a negative CD spectrum (Figure S75).

It is now necessary to understand why the CD response is just the opposite on moving the stereogenic center simply from a bound to an unbound functionality (Figure 6). It has been observed that the porphyrin ring closer to the stereogenic center sterically differentiates between the substituents at the stereogenic center. Here, because of its proximity, the second porphyrin ring has participated in steric differentiation with the chiral substrate that has a stereogenic center at the unbound functionality. Mg(II)porphyrin binds the hydroxyl group *anti* to the largest substituent on the stereogenic center and stereodifferentiates between the two groups (large and medium) that are projected to the nearest porphyrin. Here, the **1**·$(L^7_{(S)})_2$ complex is taken as a representative example in which the stereogenic center is at the unbound functionality. Chiral $L^7_{(S)}$ has an *S* conformation that gives a negative CD sign in solution, which is also supported by DFT. In the Newman projection of the amino alcohol, the stereogenic center is at the front and the CH_2OH group is at the back. Accordingly, the host porphyrin (***P1***) approaches the binding site (CH_2OH) from the side of the smallest group, S (H), keeping the large group, L (CH_2CH_3), and the medium group, M (NH_2), away. Now the large (L) and medium (M) groups are closer to the adjacent porphyrin (***P2***) and, thereby, dictate that ***P2*** rotate in an anticlockwise direction to minimize host–guest steric clash, which eventually resulted in the negative sign of the CD couplet (Figures S76 and S77). Similarly, the other enantiomer, $L^8_{(R)}$, gives a positive CD spectrum (Figures S78 and S79).

It has been observed that when the stereogenic center is at the bound functionality, the *S* substrate gives a positive and the *R* substrate a negative CD sign. However, when the stereogenic center is at the unbound functionality, the sign of the CD couplet is just the opposite; e.g., the *S* substrate gives a negative CD couplet, while the *R* substrate produces a positive CD, which is also further supported by DFT. What would happen if the substrate contained stereogenic centers at both the bound and unbound functionalities? As expected, the stereogenic center at the bound functionality dominates over the unbound one because substituents closer to the binding center will have more interactions with the adjacent porphyrin (Figure S80). The ECCD sign of a large number of substrates has followed consistent and predictable trends.

It is, however, interesting to note here that dibenzothiophene-bridged Mg(II)bisporphyrin, **1**, has been able to host a large series of 1,2-diols/amino alcohols to form 1:2 host–guest complexes that eventually allow us to accurately determine the absolute configuration of the substrate. Because of the spacer's rigidity, two porphyrin rings have little vertical flexibility, which is clearly reflected in the almost identical Mg···Mg nonbonding separation of 8.00 ± 0.02 Å and the angle (θ) between two porphyrin planes of 42.8 ± 2.0° observed in the X-ray structures (Table 1) of all the three complexes even if the bulk of the substituents on the substrate is very different. Also, Mg(II)bisporphyrin provides very little horizontal flexibility, which can be seen in the observed small torsional angles (Table 1) in the X-ray structures of the host–guest complexes reported

DOI: 10.1021/acs.joc.6b00724
J. Org. Chem. 2016, 81, 5440–5449

here. Thus, the substrate that can be fitted within the bisporphyrin cavity for 1:2 *endo-endo* complexation upon stabilization through the H-bonding interaction would lead us to an accurate stereochemical determination. Strong complexation of the substrates through alcoholic oxygen with Mg(II)bisporphyrin rigidifies the host−guest complex in which two porphyrin macrocycles have been forced to be oriented in a clockwise/anticlockwise direction to minimize the host−guest steric interactions. This has also eventually enhanced the bisignate CD signal intensity of the 1:2 host−guest complex that, otherwise, would produce negligible CD signals.

SUMMARY

In conclusion, a general, sensitive, and nonempirical protocol for determining accurate absolute configurations of a series of 1,2 diol/amino alcohols is reported here using dibenzothiophene-bridged Mg(II)bisporphyrin, **1**, as a host. Addition of excess substrates resulted in the formation of 1:2 host−guest complexes in which two substrates bind in an unusual *endo-endo* fashion within the bisporphyrin cavity, leading to the formation of unidirectional screw that allows the absolute stereochemical determination of the chiral substrate based on the observed ECCD. The sign of the CD couplet has also been found to be inverted on moving the stereogenic center by one C atom simply from the bound to the unbound functionality and thus can be used to discriminate between them. Spectroscopic investigation along with X-ray structure determination of the 1:2 host−guest complex and DFT calculations clearly support the observed CD signals and thereby assignments of the absolute stereochemistry of the chiral substrate. A large number of substrates have followed consistent and predictable trends; thus, the system is widely applicable.

EXPERIMENTAL SECTION

Materials. Enantiomerically pure chiral ligands [$L^{1}_{(S)}$−$L^{16}_{(2R,3S)}$ and $L^{20}_{(S)}$−$L^{24}_{(S)}$] were purchased from Sigma-Aldrich. Enantiopure amino alcohol $L^{17}_{(2S,3R)}$ was synthesized by esterification of L-threonine with benzyl alcohol.[21] Enantiopure amino alcohols $L^{18}_{(1R,2S)}$ and $L^{19}_{(1S,2R)}$ were synthesized from D-phenylglycine and L-phenylglycine, respectively, following the reported procedure.[22]

Synthesis. *Synthesis of* ***1***. The free base form of H_4DBT[16] (50 mg, 0.044 mmol) was taken in 20 mL of anhydrous dichloromethane; 250 μL of anhydrous triethylamine and then $MgBr_2$·OEt_2 (227 mg, 0.88 mmol) were added to it, and the mixture was stirred under a N_2 atmosphere at room temperature for 1 h. Fifty milliliters of anhydrous dichloromethane was added to the reaction mixture and the mixture washed with distilled water once. The solvent was dried over anhydrous Na_2SO_4, filtered, and evaporated to dryness. The solid residue was then purified by column chromatography on basic alumina using a dry CH_2Cl_2/acetone (1:1) eluant. Yield: 36 mg (69%). Anal. Calcd for $C_{76}H_{76}N_8S_1Mg_2$: C, 77.22; H, 6.48; N, 9.48. Found: C, 77.38; H, 6.61; N, 9.59. UV−vis (dichloromethane) [λ_{max}, nm (ε, M^{-1} cm^{-1})]: 407 (3.97×10^5), 421^{sh} (1.32×10^5), 547 (2.22×10^4), 582 (1.56×10^4). ^{1}H NMR (400 MHz, $CDCl_3$, 295 K): δ 9.68 (s, 4H, 10,20-meso-*H*), 9.63 (s, 2H, 15-meso-*H*), 8.79 (d, J = 8 Hz, 2H, Ar-*H*), 8.02 (d, J = 7.2 Hz, 2H, Ar-*H*), 7.96 (t, J = 8 Hz, 2H, Ar-H), 3.83 (m, 16H, -CH_2), 3.32 (s, 12H, -CH_3), 2.25 (s, 12H, -CH_3), 1.58 (t, J = 8.4 Hz, 12H, -CH_3). 1.48 (t, J = 8.4 Hz, 12H, -CH_3). ESI-MS: m/z 1180.5672 ([**1**]$^+$). ^{13}C NMR (400 MHz, $CDCl_3$, 295 K): δ 11.2, 11.5, 13.6, 14.0, 14.1, 17.5, 17.6, 17.8, 17.9, 19.7, 19.9, 29.9, 95.6, 96.1, 97.0, 97.3, 115.7, 116.7, 117.2, 122.0, 125.2, 131.5, 131.6, 132.2, 134.5, 135.4, 135.7, 136.3, 136.7, 137.5, 139.9, 140.4, 141.7, 142.6,144.3, 144.6, 145.9, 146.9, 148.4.

The 1:2 *endo-endo* complexes reported in this work were prepared using the general procedure; details are given below for one representative case.

1·$(L^{1}_{(S)})_2$. **1** (50 mg, 0.042 mmol) was dissolved in 5 mL of distilled dichloromethane. $L^{1}_{(S)}$ (18.0 mg, 0.24 mmol) was added to it and the mixture stirred for ∼30 min in air at room temperature. The reaction mixture was filtered off to remove any solid residue and carefully layered with dry acetonitrile. After the mixture had stood undisturbed for 6−7 days in air at room temperature, a dark crystalline solid was precipitated and was then isolated by filtration, washed with acetonitrile, and dried in vacuum. Yield: 36 mg (56%). UV−vis (dichloromethane) [λ_{max}, nm (ε, M^{-1} cm^{-1})]: 408 (3.72×10^5), 422^{sh} (1.28×10^5), 547 (2.18×10^4), 582 (1.50×10^4). ^{1}H NMR (400 MHz, $CDCl_3$, 295 K): δ 9.84 (s, 2H, 10-meso-*H*), 9.79 (s, 2H, 15-meso-*H*), 9.77 (s, 2H, 20-meso-*H*), 8.82 (d, J = 8 Hz, 2H, Ar-*H*), 8.04 (d, J = 6.8 Hz, 2H, Ar-*H*), 7.73 (t, 2H, J = 7.8 Hz, Ar-*H*), 3.92−3.81 (m, 16H, -CH_2), 3.56 (s, 6H, -CH_3), 3.53 (s, 6H, -CH_3), 2.43 (s, 6H, -CH_3), 2.40 (s, 6H, -CH_3), 1.84−1.70 (m, 24H, -CH_3), −0.23 (br, 1H, H_a), −0.37 (br, 1H, H_b), −0.90 (br, 3H, H_d), −0.90 (br, 1H, H_c), −0.91 (br, 3H, -NH_2/*OH*).

1·$(L^{3}_{(R)})_2$. Yield: 34 mg (59%). UV−vis (dichloromethane) [λ_{max}, nm (ε, M^{-1} cm^{-1})]: 409 (3.71×10^5), 422 (1.36×10^5), 548 (2.26×10^4), 582 (1.56×10^4). ^{1}H NMR (400 MHz, $CDCl_3$, 295 K): δ 9.88 (s, 2H, 10-meso-*H*), 9.78 (s, 2H, 15-meso-*H*), 9.75 (s, 2H, 20-meso-*H*), 8.81 (d, J = 8 Hz, 2H, Ar-*H*), 8.06 (d, J = 7 Hz, 2H, Ar-*H*), 8.02 (t, J = 7.8 Hz, 2H, Ar-*H*), 3.82 (m, 16H, -CH_2), 3.42 (s, 6H, -CH_3), 3.37 (s, 6H, -CH_3), 2.42 (s, 6H, -CH_3), 2.34 (s, 6H, -CH_3), 1.70−1.58 (m, 24H, -CH_3), −0.90 to −1.05 (br, 9H, H_a, H_b, H_c, H_d, H_e, H_f, *OH*/*NH*).

1·$(L^{4}_{(S)})_2$. Yield: 33 mg (54%). UV−vis (dichloromethane) [λ_{max}, nm (ε, M^{-1} cm^{-1})]: 406 (4.02×10^5), 420^{sh} (1.20×10^5), 546 (2.42×10^4), 583 (1.42×10^4). ^{1}H NMR (400 MHz, $CDCl_3$, 295 K): δ 9.72 (s, 2H, 10-meso-*H*), 9.62 (s, 2H, 15-meso-*H*), 9.62 (s, 2H, 20-meso-*H*), 8.83 (d, J = 8 Hz, 2H, Ar-*H*), 8.11 (d, J = 6.8 Hz, 2H, Ar-*H*), 7.99 (t, J = 8 Hz, 2H, Ar-*H*), 3.85 (m, 16H, -CH_2), 3.36 (s, 6H, -CH_3), 3.32 (s, 6H, -CH_3), 2.34 (s, 6H, -CH_3), 2.30 (s, 6H, -CH_3), 1.65 (m, 24H, -CH_3), 0.1 (s, 1H, -*CH*), −0.22 (s, 2H, -CH_2), −1.12 (s, 3H, -CH_3), −3.46 (br, 2H, -*OH*).

1·$(L^{5}_{(S)})_2$. Yield: 36 mg (58%). UV−vis (dichloromethane) [λ_{max}, nm (ε, M^{-1} cm^{-1})]: 409 (3.91×10^5), 422 (1.35×10^5), 547 (2.21×10^4), 583 (1.43×10^4). ^{1}H NMR (400 MHz, $CDCl_3$, 295 K): δ 9.82 (s, 2H, 10-meso-*H*), 9.71 (s, 2H, 15-meso-*H*), 9.68 (s, 2H, 20-meso-*H*), 8.82 (d, J = 7.8 Hz, 2H, Ar-*H*), 8.11 (d, J = 7.2 Hz, 2H, Ar-*H*), 8.05 (t, J = 8 Hz, 2H, Ar-*H*), 6.12 [br, 6H,Ph-H(L)], 3.84 (m, 16H, -CH_2), 3.61 [br, 4H,Ph-H(L)], 3.41 (s, 6H, -CH_3), 3.35 (s, 6H, -CH_3), 2.43 (s, 6H, -CH_3), 2.32 (s, 6H, -CH_3), 1.70−1.56 (m, 24H, -CH_3), 1.11 (br, 2H, H_a, H_b), 0.91 (br, 1H, H_c), 0.45 (br, 2H, *OH*).

1·$(L^{6}_{(S)})_2$. Yield: 37 mg (63%). UV−vis (dichloromethane) [λ_{max}, nm (ε, M^{-1} cm^{-1})]: 408 (3.86×10^5), 423 (1.25×10^5), 547 (2.24×10^4), 582 (1.52×10^4). ^{1}H NMR (400 MHz, $CDCl_3$, 295 K): δ 9.96 (s, 2H, 15-meso-*H*), 9.66 (s, 4H, 10, 20-meso-*H*), 8.65 (d, J = 8 Hz, 2H, Ar-*H*), 8.08 (d, J = 6.8 Hz, 2H, Ar-*H*), 8.01 (t, J = 8 Hz, 2H, Ar-*H*), 3.85 (m, 16H, -CH_2), 3.41 (s, 6H, -CH_3), 3.36 (s, 6H, -CH_3), 2.42 (s, 6H, -CH_3), 2.33 (s, 6H, -CH_3), 1.78−1.62 (m, 24H, -CH_3), −1.62 (br, 3H, H_d), −2.29 (br, 3H, H_a, H_b, H_c), −2.35 (br, 3H, NH_2/*OH*).

1·$(L^{7}_{(S)})_2$. Yield: 30 mg (56%). UV−vis (dichloromethane) [λ_{max}, nm (ε, M^{-1} cm^{-1})]: 410 (4.35×10^5), 422 (1.56×10^5), 547 (2.64×10^4), 584 (1.48×10^4). ^{1}H NMR (400 MHz, $CDCl_3$, 295 K): δ 9.72 (s, 4H, 10,20-meso-*H*), 9.63 (s, 2H, 15-meso-*H*), 8.80 (d, J = 8 Hz, 2H, Ar-*H*), 8.07 (d, J = 7.2 Hz, 2H, Ar-*H*), 8.01 (t, J = 8 Hz, 2H, Ar-*H*), 3.86−3.77 (m, 16H, -CH_2), 3.36 (s, 6H, -CH_3), 3.34 (s, 6H, -CH_3), 2.32 (s, 6H, -CH_3), 2.29 (s, 6H, -CH_3), 1.64−1.56 (m, 24H, -CH_3), −0.88 [br, 3H, -CH_3(L)], −2.00 (br, 2H, H_d, H_e), −2.41 (br, 1H, H_a), −2.73 (br, 1H, H_b), −3.38 (br, 1H, H_c), −3.92 (br, 3H, -NH_2/*OH*).

1·$(L^{9}_{(S)})_2$. Yield: 34 mg (52%). UV−vis (dichloromethane) [λ_{max}, nm (ε, M^{-1} cm^{-1})]: 409 (4.07×10^5), 422 (1.38×10^5), 547 (2.38×10^4), 584 (1.42×10^4). ^{1}H NMR (400 MHz, $CDCl_3$, 295 K): δ 9.86 (s, 2H, 10-meso-*H*), 9.84 (s, 2H, 15-meso-*H*), 9.82 (s, 2H, 20-meso-*H*), 8.84 (d, J = 8 Hz, 2H, Ar-*H*), 8.12 (d, J = 6.8 Hz, 2H, Ar-*H*), 8.04

DOI: 10.1021/acs.joc.6b00724
J. Org. Chem. 2016, 81, 5440−5449

Table 3. Crystal Data and Data Collection Parameters

	1·$(L^{7}_{(S)})_2$·CH_2Cl_2	**1**·$(L^{10}_{(S)})_2$·$CHCl_3$	**1**·$(L^{15}_{(2S,3R)})_2$
formula	$C_{85}H_{96}N_{10}O_2SCl_2Mg_2$	$C_{177}H_{209}N_{20}O_4S_2Cl_3Mg_4$	$C_{96}H_{112}Mg_2N_8O_4S$
T (K)	100(2)	100(2)	100(2)
formula weight	1441.30	2948.34	1522.61
crystal system	orthorhombic	monoclinic	orthorhombic
space group	$P2_12_12_1$	$P2_1$	$P2_12_12_1$
a (Å)	13.195(5)	13.376(2)	13.6073(11)
b (Å)	23.759(5)	24.659(4)	24.816(2)
c (Å)	24.771(5)	24.538(4)	25.860(2)
α (deg)	90	90	90
β (deg)	90	90.141(3)	90
γ (deg)	90	90	90
V (Å^3)	7766(4)	8094(2)	8732.5(13)
radiation [λ (Å)]	Mo Kα (0.71073)	Mo Kα (0.71073)	Mo Kα (0.71073)
Z	4	2	4
d_{calcd} (g cm^{-3})	1.233	1.210	1.158
F(000)	3064	3148	3264
crystal size	0.20 mm × 0.16 mm × 0.13 mm	0.21 mm × 0.17 mm × 0.12 mm	0.26 mm × 0.20 mm × 0.16 mm
μ (mm^{-1})	0.181	0.159	0.106
no. of unique data	14420	28130	16173
no. of restraints	4	1	0
no. of parameters, refined	955	1937	1044
GOF on F^2	1.010	1.014	1.047
R_1[a] [$I > 2\sigma(I)$]	0.0631	0.0894	0.0579
R_1[a] (all data)	0.0987	0.1551	0.0768
wR_2[b] (all data)	0.1679	0.2385	0.1522
largest difference peak and hole (e Å^{-3})	0.450 and −0.354	0.847 and −0.437	0.384 and −0.222

[a] $R_1 = (\sum||F_o| - |F_c||)/(\sum|F_o|)$. [b] $wR_2 = (\{\sum[w(F_o^2 - F_c^2)^2]\}/\{\sum[w(F_o^2)^2]\})^{1/2}$.

(t, J = 8 Hz, 2H, Ar-*H*), 6.82 [br, 2H,Ph-H(L)], 4.12 [m, 4H,Ph-H(L)], 3.88 (m, 16H, -CH_2), 3.46 (s, 6H, -CH_3), 3.40 (s, 6H, -CH_3), 2.38 (s, 6H, -CH_3), 2.32 (s, 6H, -CH_3), 1.70−1.56 (m, 24H, -CH_3), −0.40 [br, 2H, -H_d, H_e(L)], −1.78 (br, 3H, H_a, H_b, H_c), −2.70 (br, 3H, NH_2/O*H*).

1·$(L^{10}_{(S)})_2$. Yield: 36 mg (58%). ESI-MS: m/z 1315.6340 [**1**·$(L^{10}_{(S)})$ + H_2O]$^+$. UV−vis (dichloromethane) [λ_{max}, nm (ε, M^{-1} cm^{-1})]: 410 (4.40 × 10^5), 422 (1.51 × 10^5), 547 (2.58 × 10^4), 584 (1.43 × 10^4). ^{1}H NMR (400 MHz, $CDCl_3$, 295 K): δ 9.78 (s, 2H, 10-meso-*H*), 9.65 (s, 2H, 15-meso-*H*), 9.63 (s, 2H, 20-meso-*H*), 8.84 (d, J = 8 Hz, 2H, Ar-*H*), 8.09 (d, J = 7 Hz, 2H, Ar-*H*), 8.01 (t, J = 8 Hz, 2H, Ar-*H*), 3.83 (m, 16H, -CH_2), 3.39 (s, 6H, -CH_3), 3.34 (s, 6H, -CH_3), 2.44 (s, 6H, -CH_3), 2.34 (s, 6H, -CH_3), 1.70−1.56 (m, 24H, -CH_3), 0.5 [t, J = 7.5 Hz, 3H, -CH_3(L)], −1.10 (br, 1H, H_e), −1.37 (br, 1H, H_f), −1.53 [br, 3H, -CH_3(L), H_d], −2.38 (br, 1H, H_a), −2.91 (br, 1H, H_b), −3.58 (br, 1H, H_c), −4.00 (br, 3H, -NH_2/O*H*).

1·$(L^{11}_{(S)})_2$. Yield: 33 mg (54%). UV−vis (dichloromethane) [λ_{max}, nm (ε, M^{-1} cm^{-1})]: 409 (4.52 × 10^5), 421 (1.84 × 10^5), 547 (2.65 × 10^4), 584 (1.49 × 10^4). ^{1}H NMR (400 MHz, $CDCl_3$, 295 K): δ 9.98 (s, 2H, 10-meso-*H*), 9.74 (s, 2H, 15-meso-*H*), 9.45 (s, 2H, 20-meso-*H*), 8.85 (d, J = 8 Hz, 2H, Ar-*H*), 8.02 (m, 4H, Ar-*H*), 6.81 [t, J = 7.8 Hz, 2H, Ph-*H*(L)], 6.49 [m, 4H, Ph-*H*(L)], 3.98−3.84 (m, 16H, -CH_2), 3.67 [m, 4H, Ph-*H*(L)], 3.40 (s, 6H, -CH_3), 3.39 (s, 6H, -CH_3), 2.36 (s, 6H, -CH_3), 2.29 (s, 6H, -CH_3), 1.79−1.46 (m, 24H, -CH_3), −1.68 (br, 2H, H_c), −2.45 (br, 2H, H_a), −3.42 (br, 2H, H_b), −3.48 (br, 6H, -NH_2/O*H*).

1·$(L^{13}_{(R)})_2$. Yield: 27 mg (42%). UV−vis (dichloromethane) [λ_{max}, nm (ε, M^{-1} cm^{-1})]: 408 (3.88 × 10^5), 423 (1.49 × 10^5), 547 (2.54 × 10^4), 583 (1.49 × 10^4). ^{1}H NMR (400 MHz, $CDCl_3$, 295 K): δ 9.98 (s, 2H, 15-meso-*H*), 9.72 (s, 4H, 10,20-meso-*H*), 8.81 (d, J = 8 Hz, 2H, Ar-*H*), 8.11 (d, J = 6.8 Hz, 2H, Ar-*H*), 8.04 (t, J = 8 Hz, 2H, Ar-*H*), 6.81 [t, J = 7.8 Hz, 2H, Ph-*H*(L)], 6.49 [m, 4H, Ph-*H*(L)], 3.89 [m, 4H, Ph-*H*(L)], 3.81 (m, 16H, -CH_2), 3.39 (s, 6H, -CH_3), 3.34 (s, 6H, -CH_3), 2.42 (s, 6H, -CH_3), 2.36 (s, 6H, -CH_3), 1.70−1.56 (m, 24H, -CH_3), −0.67 (br, 2H, H_b,H_a), −1.01 (br, 1H, H_c), −1.53 (br, 3H, -NH_2/O*H*).

1·$(L^{14}_{(2R,3R)})_2$. Yield: 34 mg (55%). ESI-MS: m/z 1362.7146 [**1**·$(L^{14}_{(2R,3R)})_2$ + 2H]$^+$. UV−vis (dichloromethane) [λ_{max}, nm (ε, M^{-1} cm^{-1})]: 408 (3.96 × 10^5), 422^{sh} (1.18 × 10^5), 547 (2.45 × 10^4), 583 (1.42 × 10^4). ^{1}H NMR (400 MHz, $CDCl_3$, 295 K): δ 9.69 (s, 2H, 10-meso-*H*), 9.66 (s, 2H, 15-meso-*H*), 9.55 (s, 2H, 20-meso-*H*), 8.78 (d, J = 8 Hz, 2H, Ar-*H*), 8.15 (d, J = 7.2 Hz, 2H, Ar-*H*), 8.00 (t, J = 8 Hz, 2H, Ar-*H*), 3.80 (m, 16H, -CH_2), 3.39 (s, 6H, -CH_3), 3.31 (s, 6H, -CH_3), 2.32 (s, 6H, -CH_3), 2.27 (s, 6H, -CH_3), 1.60 (m, 24H, -CH_3), −2.32 (s, 2H, -C*H*), −2.88 (s, 6H, -CH_3), −3.11 (br, 2H, -O*H*).

1·$(L^{15}_{(2S,3R)})_2$. Yield: 38 mg (59%). ESI-MS: m/z 1521.8223 ([**1**·$(L^{15}_{(2S,3R)})_2$ + H]$^+$). UV−vis (dichloromethane) [λ_{max}, nm (ε, M^{-1} cm^{-1})]: 409 (3.99 × 10^5), 422^{sh} (7.64 × 10^4), 548 (2.14 × 10^4), 580 (1.45 × 10^4). ^{1}H NMR (400 MHz, $CDCl_3$, 295 K): δ 9.79 (s, 2H, 10-meso-*H*), 9.67 (s, 2H, 15-meso-*H*), 9.62 (s, 2H, 20-meso-*H*), 8.81 (d, J = 8 Hz, 2H, Ar-*H*), 8.06 (d, J = 6.8 Hz, 2H, Ar-*H*), 7.99 (t, J = 7.6 Hz, 2H, Ar-*H*), 3.82 (m, 16H, -CH_2), 3.38 (s, 6H, -CH_3), 3.34 (s, 6H, -CH_3), 2.29 (s, 6H, -CH_3), 2.27 (s, 6H, -CH_3), 1.66 (m, 24H, -CH_3), 0.72 [br, 18H, -CH_3(L)], 0.45 (br, 8H, L-*H*), −1.00 (br, 8H, L-*H*), −1.82 [br, 2H, -O*H*(L)].

1·$(L^{17}_{(2S,3R)})_2$. Yield: 34 mg (58%). UV−vis (dichloromethane) [λ_{max}, nm (ε, M^{-1} cm^{-1})]: 409 (3.72 × 10^5), 423 (1.53 × 10^5), 547 (2.60 × 10^4), 583 (1.43 × 10^4). ^{1}H NMR (400 MHz, $CDCl_3$, 295 K): δ 9.79 (s, 2H, 10-meso-*H*), 9.73 (s, 2H, 15-meso-*H*), 9.71 (s, 2H, 20-meso-*H*), 8.82 (d, J = 8 Hz, 2H, Ar-*H*), 8.04 (d, J = 6.4 Hz, 2H, Ar-*H*), 8.01 (t, J = 7.2 Hz, 2H, Ar-*H*), 7.34 [t, J = 7.8 Hz, 3H, Ph-*H*(L)], 6.23 [m, 2H, Ph-*H*(L)], 3.83 (m, 16H, -CH_2), 3.44 (s, 6H, -CH_3), 3.34 (s, 6H, -CH_3), 2.44 (s, 6H, -CH_3), 2.34 (s, 6H, -CH_3), 1.92 [s, 2H, CH_2(L)], 1.70−1.56 (m, 24H, -CH_3), −0.60 [br, 2H, -CH_2(H_d)], −1.70 (d, 2H, H_c), −2.55 (br, 2H, H_a, H_b), −3.29 (br, 3H, -NH_2/O*H*).

1·$(L^{18}_{(1R,2S)})_2$. Yield: 38 mg (56%). ESI-MS: m/z 1315.6340 ([$L^{18}_{(1R,2S)}$ + H_2O]$^+$). UV−vis (dichloromethane) [λ_{max}, nm (ε, M^{-1} cm^{-1})]: 409 (4.06 × 10^5), 423 (1.54 × 10^5), 547 (2.62 × 10^4), 582 (1.53 × 10^4). ^{1}H NMR (400 MHz, $CDCl_3$, 295 K): δ 9.88 (s, 2H, 10-meso-*H*), 9.85 (s, 2H, 15-meso-*H*), 9.82 (s, 2H, 20-meso-*H*), 8.88 (d, J = 8 Hz, 2H, Ar-*H*), 8.09 (d, J = 6.8 Hz, 2H, Ar-*H*), 8.01 (t, J = 8 Hz,

DOI: 10.1021/acs.joc.6b00724
J. Org. Chem. 2016, 81, 5440−5449

2H, Ar-*H*), 6.56 [t, *J* = 7.8 Hz, 2H, Ph-*H*(L)], 6.23 [m, 4H, Ph-*H*(L)], 3.86 [m, 4H, Ph-*H*(L)], 3.83 (m, 16H, -CH_2), 3.39 (s, 6H, -CH_3), 3.34 (s, 6H, -CH_3), 2.43 (s, 6H, -CH_3), 2.33 (s, 6H, -CH_3), 1.72−1.58 (m, 24H, -CH_3), −0.6 (br, 3H, H_c), −1.71 (d, 2H, H_b), −2.22 (br, 3H, -NH_2/OH).

X-ray Structure Solution and Refinement. Slow evaporation of acetonitrile into the dichloromethane solution of **1**·$(L^7_{(S)})_2$, **1**·$(L^{15}_{(2S,3R)})_2$ and chloroform solution of **1**·$(L^{10}_{(S)})_2$ in air at room temperature gave dark red crystals. Crystals were coated with light hydrocarbon oil and mounted in the 100 K dinitrogen stream, and intensity data were collected using graphite-monochromated Mo Kα radiation (λ = 0.71073 Å). Integration and reduction of data were processed with SAINT.[23] An absorption correction was applied.[24] Structures were determined by the direct method using SHELXS-97 and were refined on F^2 by the full-matrix least-squares technique using the SHELXL-2014 program package.[25] Non-hydrogen atoms were refined anisotropically. In the refinement, hydrogens were treated as riding atoms using SHELXL default parameters. Crystallographic data and data collection parameters are listed in Table 3.

CCDC entries 1448120 [**1**·$(L^7_{(S)})_2$], 1448121 [**1**·$(L^{10}_{(S)})_2$], and 1017376 [**1**·$(L^{15}_{(2S,3R)})_2$] contain the supplementary crystallographic data for this paper. These data can be obtained free of charge from the Cambridge Crystallographic Data Center via www.ccdc.cam.ac.uk/data_request/cif.

Computational Details. DFT calculations were performed by employing a B3LYP hybrid functional using the Gaussian 09, revision B.01, package.[26] The method used included Becke's three-parameter hybrid exchange functional,[27] the nonlocal correlation provided by the Lee, Yang, and Parr expression,[28] and the Vosko, Wilk, and Nussair 1980 correlation functional (III) for local correction. The basis sets were LANL2DZ for Mg and S and 6-31G+(d,p) for C, N, O, and H. Full geometry optimizations of all the complexes were conducted in dichloromethane taking the coordinates from the crystal structures. Dispersion corrections were not implemented as the increased attractive forces led to unreasonable porphyrin ring distances.

Processing of the TDDFT calculations and comparison with the experimental spectrum were performed with SpecDis.[29] The following CD shifts and σ values were used: 60 nm and 0.04 eV for **1**·$(L^1_{(S)})_2$, **1**·$(L^2_{(R)})_2$, **1**·$(L^7_{(S)})_2$, and **1**·$(L^8_{(R)})_2$ and 66 nm and 0.06 eV for **1**·$(L^{15}_{(2S,3R)})_2$ and **1**·$(L^{15}_{(2S,3S)})_2$, respectively, where chirality has been changed manually.

■ ASSOCIATED CONTENT

Supporting Information

The Supporting Information is available free of charge on the ACS Publications website at DOI: 10.1021/acs.joc.6b00724.

DFT-optimized structures, Figures S1−S80, and Tables S1 and S2 (PDF)

Crystallographic data for **1**·$(L^7_{(S)})_2$ (CIF)

Crystallographic data **1**·$(L^{10}_{(S)})_2$(CIF)

Crystallographic data **1**·$(L^{15}_{(2S,3R)})_2$(CIF)

■ AUTHOR INFORMATION

Corresponding Author

*E-mail: sprath@iitk.ac.in.

Notes

The authors declare no competing financial interest.

■ ACKNOWLEDGMENTS

We thank the Council of Scientific and Industrial Research (CSIR), New Delhi, and the Science and Engineering Research Board (SERB) for financial support. CARE scheme of IIT Kanpur is gratefully acknowledged for the CD facility.

■ REFERENCES

(1) (a) van Dijken, D. J.; Beierle, J. M.; Stuart, M. C. A.; Szymański, W.; Browne, W. R.; Feringa, B. L. *Angew. Chem., Int. Ed.* **2014**, *53*, 5073. (b) Schwartz, E.; La Gac, S.; Cornelissen, J. L. M. J.; Nolte, R. J. M.; Rowan, A. E. *Chem. Soc. Rev.* **2010**, *39*, 1576. (c) Palmans, A. R. A.; Meijer, E. W. *Angew. Chem., Int. Ed.* **2007**, *46*, 8948.

(2) (a) Sato, K.; Itoh, Y.; Aida, T. *Chem. Sci.* **2014**, *5*, 136. (b) Ohta, I.; Sato, H.; Ando, S.; Kosaka, A.; Fukushima, T.; Hashizume, D.; Yamasaki, M.; Hasegawa, K.; Muraoka, A.; Ushiyama, H.; Yamashita, K.; Aida, T. *Nat. Chem.* **2011**, *3*, 68.

(3) (a) Bentley, K. W.; Wolf, C. *J. Am. Chem. Soc.* **2013**, *135*, 12200. (b) Dong, Z.; Karpowicz, R. J., Jr.; Bai, S.; Yap, G. P. A.; Fox, J. M. *J. Am. Chem. Soc.* **2006**, *128*, 14242. (c) Harmata, M. *Acc. Chem. Res.* **2004**, *37*, 862.

(4) (a) Yamamoto, S.; Iida, H.; Yashima, E. *Angew. Chem., Int. Ed.* **2013**, *52*, 6849. (b) Akine, S.; Sairenji, S.; Taniguchi, T.; Nabeshima, T. *J. Am. Chem. Soc.* **2013**, *135*, 12948.

(5) (a) Joyce, L.; Maynor, M.; Dragna, J.; da Cruz, G. M.; Lynch, V.; Canary, J. W.; Anslyn, E. V. *J. Am. Chem. Soc.* **2011**, *133*, 13746. (b) Canary, J. W. *Chem. Soc. Rev.* **2009**, *38*, 747. (c) Canary, J. W.; Mortezaei, S.; Liang, J. *Coord. Chem. Rev.* **2010**, *254*, 2249.

(6) (a) Nakanishi, K.; Berova, N.; Woody, R. W. *Circular Dichroism: Principles and Applications*, 2nd ed.; Wiley-VCH: New York, 2000. (b) Fasman, G. D. *Circular Dichroism and the Conformational Analysis of Biomolecules*; Plenum Press: New York, 1996.

(7) (a) Pescitelli, G.; Di Bari, L.; Berova, N. *Chem. Soc. Rev.* **2014**, *43*, 5211. (b) Berova, N.; Pescitelli, G.; Petrovic, A. G.; Proni, G. *Chem. Commun.* **2009**, 5958. (c) Berova, N.; Di bari, L.; Pescitelli, G. *Chem. Soc. Rev.* **2007**, *36*, 914.

(8) (a) Borovkov, V. V.; Inoue, Y. *Eur. J. Org. Chem.* **2009**, *2009*, 189. (b) Hembury, G. A.; Borovkov, V. V.; Inoue, Y. *Chem. Rev.* **2008**, *108*, 1. (c) Borovkov, V. V.; Hembury, G. A.; Inoue, Y. *Acc. Chem. Res.* **2004**, *37*, 449. (d) Borovkov, V. V.; Fujii, I.; Muranaka, A.; Hembury, G. A.; Tanaka, T.; Ceulemans, A.; Kobayashi, N.; Inoue, Y. *Angew. Chem., Int. Ed.* **2004**, *43*, 5481. (e) Borovkov, V. V.; Lintuluoto, J. M.; Hembury, G. A.; Sugiura, M.; Arakawa, R.; Inoue, Y. *J. Org. Chem.* **2003**, *68*, 7176. (f) Lintuluoto, J. M.; Borovkov, V. V.; Inoue, Y. *J. Am. Chem. Soc.* **2002**, *124*, 13676.

(9) (a) Anyika, A.; Gholami, H.; Ashtekar, K. D.; Acho, R.; Borhan, B. *J. Am. Chem. Soc.* **2014**, *136*, 550. (b) Tanasova, M.; Borhan, B. *Eur. J. Org. Chem.* **2012**, *2012*, 3261.

(10) (a) Ikbal, S. A.; Brahma, S.; Rath, S. P. *Chem. Commun.* **2015**, *51*, 895. (b) Ikbal, S. A.; Brahma, S.; Rath, S. P. *Chem. Commun.* **2014**, *50*, 14037. (c) Brahma, S.; Ikbal, S. A.; Dhamija, A.; Rath, S. P. *Inorg. Chem.* **2014**, *53*, 2381. (d) Brahma, S.; Ikbal, S. A.; Rath, S. P. *Inorg. Chem.* **2014**, *53*, 49. (e) Brahma, S.; Ikbal, S. A.; Dey, S.; Rath, S. P. *Chem. Commun.* **2012**, *48*, 4070. (f) Ikbal, S. A.; Saha, B.; Rath, S. P. *J. Indian Chem. Soc.* **2015**, *92*, 2001.

(11) (a) Pintre, I. C.; Pierrefixe, S.; Hamilton, A.; Valderrey, V.; Bo, C.; Ballester, P. *Inorg. Chem.* **2012**, *51*, 4620. (b) Etxebarria, J.; Vidal-Ferran, A. V.; Ballester, P. *Chem. Commun.* **2008**, 5939.

(12) (a) Hayashi, S.; Yotsukura, M.; Noji, M.; Takanami, T. *Chem. Commun.* **2015**, *51*, 11068. (b) Jiang, J.; Fang, X.; Liu, B.; Hu, C. *Inorg. Chem.* **2014**, *53*, 3298. (c) D'Urso, A.; Nicotra, P. F.; Centonze, G.; Fragalá, M. E.; Gattuso, G.; Notti, A.; Pappalardo, A.; Pappalardo, S.; Parisi, M. F.; Purrello, R. *Chem. Commun.* **2012**, *48*, 4046.

(13) (a) Petrovic, A. G.; Chen, Y.; Pescitelli, G.; Berova, N.; Proni, G. *Chirality* **2010**, *22*, 129. (b) Huang, X.; Fujioka, N.; Pescitelli, G.; Koehn, F. E.; Williamson, R. T.; Nakanishi, K.; Berova, N. *J. Am. Chem. Soc.* **2002**, *124*, 10320. (c) Kurtán, T.; Nesnas, N.; Koehn, F. E.; Li, Y. Q.; Nakanishi, K.; Berova, N. *J. Am. Chem. Soc.* **2001**, *123*, 5974. (d) Huang, X.; Rickman, B. H.; Borhan, B.; Berova, N.; Nakanishi, K. *J. Am. Chem. Soc.* **1998**, *120*, 6185.

(14) (a) Li, X.; Burrell, C. E.; Staples, R. J.; Borhan, B. *J. Am. Chem. Soc.* **2012**, *134*, 9026. (b) Li, X.; Tanasova, M.; Vasileiou, C.; Borhan, B. *J. Am. Chem. Soc.* **2008**, *130*, 1885. (c) Li, X.; Burrell, C. E.; Staples, R. J.; Borhan, B. *J. Am. Chem. Soc.* **2012**, *134*, 9026. (d) Li, X.; Borhan, B. *J. Am. Chem. Soc.* **2008**, *130*, 16126.

DOI: 10.1021/acs.joc.6b00724
J. Org. Chem. 2016, 81, 5440−5449

(15) (a) Tanasova, M.; Anyika, M.; Borhan, B. *Angew. Chem., Int. Ed.* **2015**, *54*, 4274. (b) Yang, Q.; Olmsted, C.; Borhan, B. *Org. Lett.* **2002**, *4*, 3423. (c) Proni, G.; Pescitelli, G.; Huang, X.; Quraishi, N. Q.; Nakanishi, K.; Berova, N. *Chem. Commun.* **2002**, 1590.
(16) Faure, S.; Stern, C.; Guilard, R.; Harvey, P. D. *J. Am. Chem. Soc.* **2004**, *126*, 1253.
(17) (a) www.hyperquad.co.uk/HypSpec.htm. (b) Gans, P.; Sabatini, A.; Vacca, A. *Talanta* **1996**, *43*, 1739.
(18) (a) Mondal, P.; Rath, S. P. *Chem. - Eur. J.* **2016**, *22*, 5607. (b) Mondal, P.; Rath, S. P. *Eur. J. Inorg. Chem.* **2015**, *2015*, 4956. (c) Mondal, P.; Rath, S. P. *Isr. J. Chem.* **2016**, *56*, 144. (d) Mondal, P.; Chaudhary, A.; Rath, S. P. *Dalton Trans.* **2013**, *42*, 12381. (e) Chaudhary, A.; Rath, S. P. *Chem. - Eur. J.* **2012**, *18*, 7404. (f) Chaudhary, A.; Rath, S. P. *Chem. - Eur. J.* **2011**, *17*, 11478. (g) Chaudhary, A.; Patra, R.; Rath, S. P. *Indian J. Chem.* **2011**, *50A*, 1436. (h) Sil, D.; Rath, S. P. *Dalton Trans.* **2015**, *44*, 16195. (i) Dey, S.; Rath, S. P. *Dalton Trans.* **2014**, *43*, 2301.
(19) (a) Ikbal, S. A.; Dhamija, A.; Rath, S. P. *Chem. Commun.* **2015**, *51*, 14107. (b) Chaudhary, A.; Ikbal, S. A.; Brahma, S.; Rath, S. P. *Polyhedron* **2013**, *52*, 761. (c) Brahma, S.; Ikbal, S. A.; Rath, S. P. *Inorg. Chim. Acta* **2011**, *372*, 62. (d) Ikbal, S. A.; Brahma, S.; Dhamija, A.; Rath, S. P. *J. Chem. Sci.* **2014**, *126*, 1451. (e) Ikbal, S. A.; Brahma, S.; Rath, S. P. *Inorg. Chem.* **2012**, *51*, 9666.
(20) Eilei, E. L.; Wilen, S. H. *Stereochemistry of Organic Compounds*; Wiley: New York, 1994.
(21) Gutmann, H. R.; Chang, S. F. *J. Org. Chem.* **1962**, *27*, 2248.
(22) Reetz, M. T.; Drewes, M. W.; Schmitz, A. *Angew. Chem., Int. Ed. Engl.* **1987**, *26*, 1141.
(23) *SAINT+*, version 6.02; Bruker AXS: Madison, WI, 1999.
(24) Sheldrick, G. M. *SADABS*, version 2.0; 2000.
(25) Sheldrick, G. M. *SHELXL-2014: Program for Crystal Structure Refinement*; University of Göttingen: Göttingen, Germany, 2014.
(26) Frisch, M. J.; Trucks, G. W.; Schlegel, H. B.; Scuseria, G. E.; Robb, M. A.; Cheeseman, J. R.; Scalmani, G.; Barone, V.; Mennucci, B.; Petersson, G. A.; Nakatsuji, H.; Caricato, M.; Li, X.; Hratchian, H. P.; Izmaylov, A. F.; Bloino, J.; Zheng, G.; Sonnenberg, J. L.; Hada, M.; Ehara, M.; Toyota, K.; Fukuda, R.; Hasegawa, J.; Ishida, M.; Nakajima, T.; Honda, Y.; Kitao, O.; Nakai, H.; Vreven, T.; Montgomery, J. A., Jr.; Peralta, J. E.; Ogliaro, F.; Bearpark, M.; Heyd, J. J.; Brothers, E.; Kudin, K. N.; Staroverov, V. N.; Keith, T.; Kobayashi, R.; Normand, J.; Raghavachari, K.; Rendell, A.; Burant, J. C.; Iyengar, S. S.; Tomasi, J.; Cossi, M.; Rega, N.; Millam, J. M.; Klene, M.; Knox, J. E.; Cross, J. B.; Bakken, V.; Adamo, C.; Jaramillo, J.; Gomperts, R.; Stratmann, R. E.; Yazyev, O.; Austin, A. J.; Cammi, R.; Pomelli, C.; Ochterski, J. W.; Martin, R. L.; Morokuma, K.; Zakrzewski, V. G.; Voth, G. A.; Salvador, P.; Dannenberg, J. J.; Dapprich, S.; Daniels, A. D.; Farkas, O.; Foresman, J. B.; Ortiz, J. V.; Cioslowski, J.; Fox, D. J. *Gaussian 09*, revision B.01; Gaussian, Inc.: Wallingford, CT, 2010.
(27) Becke, A. D. J. *J. Chem. Phys.* **1993**, *98*, 5648.
(28) Lee, C.; Yang, W.; Parr, R. G. *Phys. Rev. B: Condens. Matter Mater. Phys.* **1988**, *37*, 785.
(29) (a) Bruhn, T.; Hemberger, Y.; Schaumlçffel, A.; Bringmann, G. *Specdis*, version 1.62; University of Wurzburg: Wurzburg, Germany, 2012. (b) Bruhn, T.; Schaumlöffel, A.; Hemberger, Y.; Bringmann, G. *Chirality* **2013**, *25*, 243.

DOI: 10.1021/acs.joc.6b00724
J. Org. Chem. 2016, 81, 5440−5449